Arnold Schwarzenegger
Governor

COASTAL IMPACTS OF NORTH PACIFIC WINTER WAVE CLIMATE VARIABILITY: THE SOUTHERN CALIFORNIA BIGHT AND THE GULF OF THE FARALLONES

PIER PROJECT REPORT

Prepared For:
California Energy Commission
Public Interest Energy Research Program

Prepared By:
Scripps Institution of Oceanography

March 2005
CEC-500-2005-018

California Climate Change Center
Report Series Number 2005-008

Prepared By:
Nicholas E. Graham
Scripps Institution of Oceanography and Hydrologic Research Center
San Diego, California

Contract No. 500-02-004
Work Authorization No. MR-004

Prepared For:
California Energy Commission
Public Interest Energy Research (PIER) Program

Guido Franco,
Contract Manager

Kelly Birkinshaw,
Program Area Team Lead
Energy-Related Environmental Research

Ron Kukulka,
Acting Deputy Director
ENERGY RESEARCH AND DEVELOPMENT DIVISION

Robert L. Therkelsen
Executive Director

Acknowledgements

This work was funded by a grant (contract number 500-02-004, Work Authorization MR-004) from the California Energy Commission to the Scripps Institution of Oceanography, by Pacific Weather Analysis and the Hydrologic Research Center. H. Tolman provided assistance and advice for the large-scale wave modeling, and W. O'Reilly generously provided the refraction model used for the downscaling.

Please cite this report as follows:

Graham, N. E.. 2005. *Coastal Impacts of North Pacific Winter Wave Climate Variability: The Southern California Bight and the Gulf of the Farallones.* Scripps Institution of Oceanography, for the California Energy Commission, PIER Energy-Related Environmental Research. CEC-500-2005-018.

Preface

The Public Interest Energy Research (PIER) Program supports public interest energy research and development that will help improve the quality of life in California by bringing environmentally safe, affordable, and reliable energy services and products to the marketplace.

The PIER Program, managed by the California Energy Commission (Energy Commission), annually awards up to $62 million to conduct the most promising public interest energy research by partnering with Research, Development, and Demonstration (RD&D) organizations, including individuals, businesses, utilities, and public or private research institutions.

PIER funding efforts are focused on the following RD&D program areas:

- Buildings End-Use Energy Efficiency
- Energy Innovations Small Grant Program
- Energy-Related Environmental Research
- Energy Systems Integration Environmentally Preferred Advanced Generation
- Industrial/Agricultural/Water End-Use Energy Efficiency
- Renewable Energy Technologies

The California Climate Change Center (CCCC) is sponsored by the PIER program and coordinated by its Energy-Related Environmental Research area. The Center is managed by the California Energy Commission, Scripps Institution of Oceanography at the University of California at San Diego, and the University of California at Berkeley. The Scripps Institution of Oceanography conducts and administers research on climate change detection, analysis, and modeling; and the University of California at Berkeley conducts and administers research on economic analyses and policy issues. The Center also supports the Global Climate Change Grant Program, which offers competitive solicitations for climate research.

The California Climate Change Center Report Series details ongoing Center-sponsored research. As interim project results, these reports receive minimal editing, and the information contained in these reports may change; authors should be contacted for the most recent project results. By providing ready access to this timely research, the Center seeks to inform the public and expand dissemination of climate change information; thereby leveraging collaborative efforts and increasing the benefits of this research to California's citizens, environment, and economy.

The work described in this report was conducted under the Preliminary Climatic Data Collection, Analyses, and Modeling contract, contract number 500-02-004, Work Authorization MR-004, by the Scripps Institution of Oceanography.

For more information on the PIER Program, please visit the Energy Commission's Web site www.energy.ca.gov/pier/ or contract the Energy Commission at (916) 654-4628.

Table of Contents

Abstract

Changes in wave climate are of interest from many perspectives, such as coastal management, near-shore engineering, sediment transport and beach erosion, and maritime safety. Results from wave hindcast simulations driven with reanalysis winds (Graham and Diaz, 2001; Wang and Swail, 2001) indicate considerable variability in North Pacific winter wave climate during the latter half of the twentieth century. Over the eastern North Pacific off the U.S. west coast, this variability (for both average and extreme waves) is dominated by a trend towards larger, longer period waves with more westerly approach directions. These changes are closely linked to changes in preferred storm tracks associated with the El Niño-Southern Oscillation and Pacific inter-decadal variability. In this paper, we review some of the open ocean hindcast results as they relate to the California coast, and examine the impacts wave climate variability in two coastal regions (the Southern California Bight and the Gulf of the Farallones) as seen in the results of downscaling simulations in which the effects of inshore sheltering and refraction are resolved. The results reveal a rich variety of wave climate change in inshore waters resulting from interactions between of the character of deep water wave climate changes and coastal wave transformations.

1. Introduction

Multi-decade wave hindcast results (Wang and Swail, 2001; Graham and Diaz, 2001) reveal considerable variability in extreme winter wave climate over the North Pacific over the past four to five decades of the twentieth century. Important aspects of these changes are related to variability in large-scale atmospheric circulation associated with El Niño activity [the El Niño-Southern Oscillation (ENSO)] at interannual time scales and with multi-decadal variability often referred to as the Pacific Decadal Oscillation (PDO). Numerous useful references discuss these modes of atmospheric variability and their expression over the North Pacific (e.g., Gutzler and Wallace, 1981); Trenberth and Hurrell, 1994; Mantua et al., 1997), while Wang and Swail (2001; cf. Bromirski et al., 2004; Allan and Komar, 2000) specifically relate changes in seasonal mean circulation changes to wave climate variability. Examining causes in changes of wave climate from a more synoptic viewpoint, Graham and Diaz (2001) document trends in winter North Pacific cyclones during the latter half of the twentieth century, noting a tendency towards increasingly vigorous systems traveling along storm tracks displaced to the south and east; changes intimately linked with the changes in seasonal mean circulation. These changes in storm strength and track had major effects on deep water wave climate (height, dominant period, and direction) off California, aspects of which are documented in some of the citations above, and reviewed in this paper.

A principal motivation for studying wave climate variability is to characterize and quantify its manifestations in inshore waters and on the shoreline. This requires accounting for the effects of coastal morphology and near-shore bathymetry on the offshore wave field, generally at relatively fine spatial scales. Here, we explore how variability in deep water winter wave climate over the Northeast Pacific described above was expressed in over two important regions along the California coast: (1) the Southern California Bight, and (2) the Gulf of the Farallones (off the San Francisco area). The analysis is performed by transforming 3-hourly deep water directional wave spectra (from the 50-year wave hindcast described by Graham and Diaz, 2001) into coastal waters using gridded (approximately 5-km resolution) transform functions (calculated using the model of O'Reilly, 1991) to account for the effects of sheltering

and refraction. The results, summarized in terms of trends and correlations for the inshore wave fields, reveal considerable spatial structure in the relationships with large-scale wave climate variability that may be useful in understanding regional patterns of shoreline change.

The presentation is organized as follows: Section 2 gives a brief description of the models and methods used; Section 3 presents a discussion of the changes in deep water North Pacific wave climate, then describes the results for the coastal regions; and Section 4 gives a brief summary.

2. Models and Methods

The ocean wave hindcast data come from a 50-year simulation conducted by Pacific Weather Analysis using the National Oceanographic and Atmospheric Administration (NOAA) National Centers for Environmental Prediction (NCEP) WAVEWATCH III model, Version 1.18 (Tolman, 1999). The model was configured at a resolution of 1.5˚ latitude and 2˚ longitude covering the North Pacific from 150˚E to the coast of North America and from 20˚N to the Aleutian Islands and Alaskan coast. A uniform ocean depth of 5000 meters (deep water) was specified at all ocean nodes in the wave model domain. Six-hourly 10-m winds from the NCEP reanalysis project (Kalnay et al., 1997) were used as forcing (as did the 40-year hindcast of Wang and Swail, 2000). The model used 5° directional resolution (72 bins) and 20 logarithmically frequency bins covering the period range from 4.4 to 27.2 seconds [the relatively fine directional resolution (a typical value for large-scale hindcasts is 15˚) was chosen to allow for more accurate transformation of hindcast results into regions of complex coastal geometry]. The simulations cover December–March (DJFM) 1948–1949 to 1997–1998; the first few days of December for each year were discarded to allow for spin-up. Model output was obtained at 3-hour intervals, giving gridded fields of significant wave height, dominant wave period, and dominant wave direction, as well as directional spectra at specified points—many of them at NOAA wave measurement buoy locations.

Although comparisons between model hindcasts and buoy measurements (shown later) show good agreement, some of the limiting factors affecting hindcast performance should be recognized, and are listed below.

1) The reanalysis winds for the hindcasts (beyond general uncertainties) are known to be biased low along the Central California coast due to the poor depiction of coastal topography at the approximately 1.8˚ resolution of the model. Strong northwest winds along this stretch of coast, though more prevalent in spring and summer, are an important factor in the winter wave climate, and occasionally make substantial contributions to wave height during episodes of high waves, so the result is a negative bias in wave energy propagating from the northwest along the coast of Central California coast and propagating through the outer waves of the Southern California Bight. This bias is most apparent at wave period less than 10–12 seconds (author's analyses).

2) The relatively coarse depiction of the California coastline at the 1.0˚ x 1.5˚ resolution of the large-scale wave model (e.g., Fig. 3a) probably results in some attenuation of wave energy propagating more or less parallel to the coast of North America, an effect believed to be most important along the Central and Southern California coasts where much of the wave energy comes west-northwest to northwest. The effect would be some reduction in wave energy approaching from the northwest at grid points adjacent to the coast of central California (and southward) and offshore of the Southern California Bight.

3) The use of only 20 frequency bands (a selection based on run-time considerations) contributed to a negative bias in the simulated wave heights, particularly during low wind - low wave conditions, and otherwise probably had minor adverse affect on the results.

4) A coding error in the model affected wave generation during periods of very low waves. The impacts of this problem on hindcast performance were similar to

those for point 3) above, and tests show some minor negative impact on the results during high wave events.

5) The placement of the western boundary at 150˚E makes it impossible to interpret the results in the far western Pacific; however, this problem has essentially no effect on large wave episodes in the eastern Pacific.

Comparisons of the hindcast results with observations from nearby NOAA wave buoys (available from the late 1970s and early 1980s) show good agreement with respect to both specific events and interannual variability, with correlations for contemporaneous 3-hourly measured and hindcast significant wave heights (H_S) of 0.85 to 0.88 for NOAA National Data Buoy Center (NDBC) wave buoys in the eastern North Pacific. This agreement is apparent in scatter plots (Fig. 1) of measured *vs.* observed significant wave height (H_S) for the locations in the eastern and central North Pacific listed in Table 1. The correlations for these points are 0.85 (Pt. Arguello), 0.88 (Pt. Reyes), 0.87 (Buoy 46006), and 0.81 (NW Hawaii; correlations for Buoy 46029 off the Oregon-Washington border (not shown) are 0.82).

Some comments concerning features on the scatter plots are given below.

A) The negative bias for low wave heights at all locations is due to the coding error and limited frequency resolution noted in the paragraph above (points 3 and 4).

B) The consistent negative bias at Pt. Arguello (indicating an 25%–30% low bias in wave energy) results from contributions from points 1–3 in the paragraph above. Because the energy deficit is in the northwesterly sector (this effect is quite apparent in Fig 11d in Graham and Diaz (2001), in years in which waves approaching from the west make large contributions to extreme H_S, the bias is

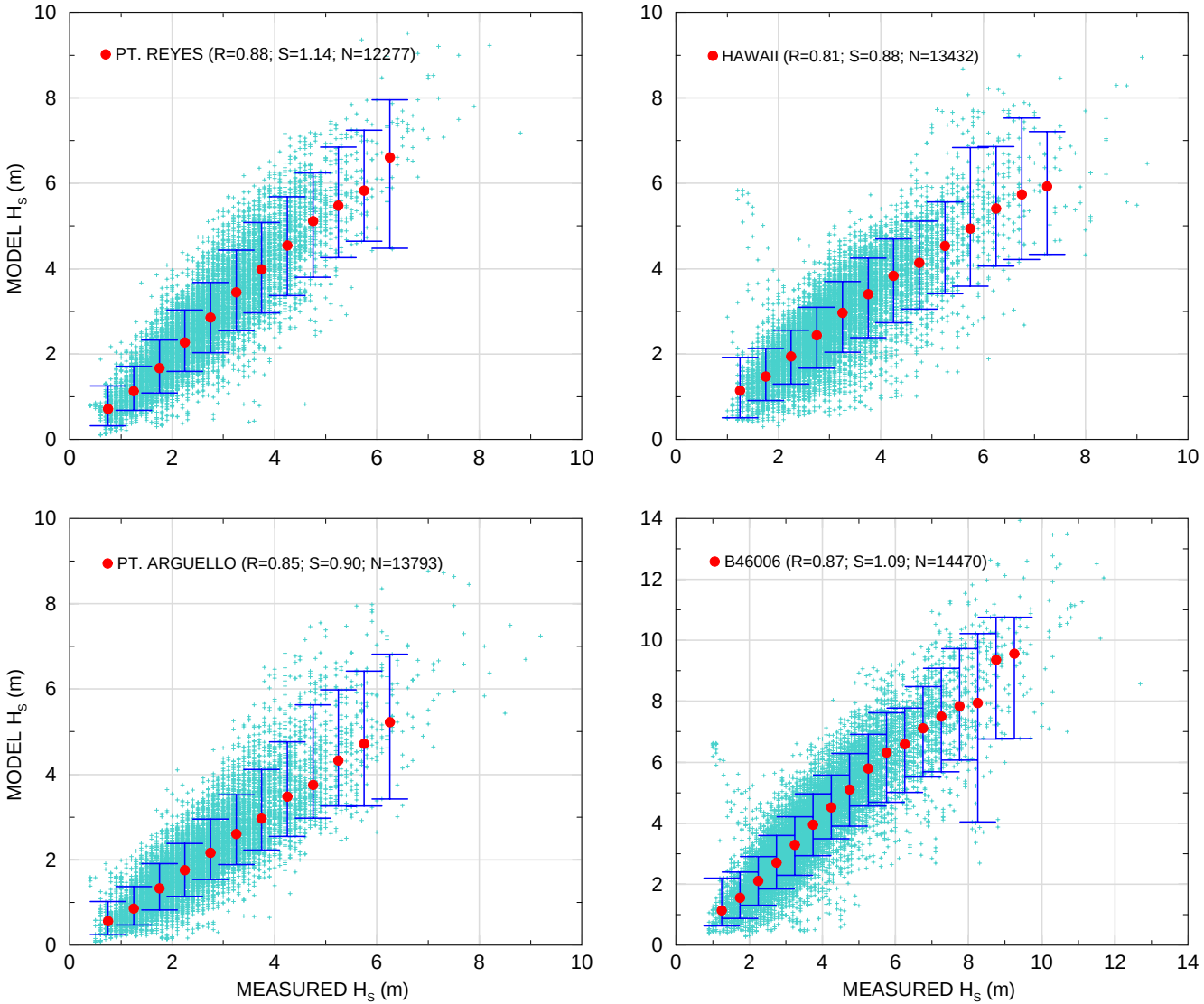

FIG. 1

Figure. Scatter plots of contemporaneous 3-hourly H_S from the NOAA buoy and hindcast results for the locations listed in Table 1. Error bars show median (circle) and 80% bounds of the model data for 0.5 m H_S bins of the measured data. Legends give correlation between measurements and hindcast data, linear least-square slope of regression of hindcast data on measurements, and number of measurement/hindcast pairs.

small), the bias has negligible effect on estimates of extreme waves in the inner waters of the Southern California Bight (SCB), which are largely protected from open ocean waves approaching from the northwest. Nevertheless, to make the results more representative for the outer waters of the SCB, we have applied a frequency-direction correction (developed in other work for sites in the outer SCB) to the Pt. Arguello spectra prior to using them with the refraction model as described below. The effects of these corrections are negligible in the inner waters of the Bight but increase the trends in the outer waters of the Bight.

Table 1. Model / Buoy Comparison Locations

DESIGNATION	MODEL LOC.	BUOY NUMBER	BUOY LOCATION	BEGINNING YEAR
Pt. Arguello	35N, 121.5W	46011	34.9N, 121.9W	1982
Pt. Reyes	38N, 124.5W	46026	37.8, 122.8	1980
B46006	41N, 138W	46006	40.9N, 137.5W	1977
NW Hawaii	23N, 162W	51001	23.4N, 162.2W	1981

Deep water wave conditions were transformed into shallow water over two domains covering the Southern California Bight (SCB; 32˚–35˚N, 117˚–121˚W) and the Gulf of the Farallones (GoF; 37.0˚–38.5˚N, 123.5˚–122.2˚W. Gridded bathymetric data for the SCB (Fig. 2a) were derived from National Ocean Survey (NOS) as described in O'Reilly (1991). For the GoF domain (Fig 2b), depths were taken from NOS soundings and from marine navigation charts. These point data were interpolated using the cubic-spline package of P. Sakov (http://www.marine.csiro.au/~sakov; c.f. Haber et al., 2001), then lightly smoothed. Grid resolution over both domains is approximately 100 m. Gridded shallow water transformation functions were calculated over each domain at a resolution of 3 minutes latitude and longitude (approximately 5 km) using the linear back-refraction model of O'Reilly (1991). These functions define the transformations $g(f,\theta) = E_S / E_0$, and $h(f,\theta) = \theta_S$, where f and θ are a given deep water frequency and direction pair, E_0 is the deep water energy for the f, θ bin, and E_S and θ_S are the shallow water energy and direction after transformation to a given point. The transformation

functions were calculated at gridded latitude-longitude coordinates, and, beyond the effects of some mild smoothing implemented in the refraction model, are (at least formally) representative of points, rather than area-averages. For both domains, transformation functions were calculated only for depths greater than 5 m. Values of E_S / E_0 were limited to 4.0 (so that the traditional refraction coefficient K_R is limited to 2.0).

The wave hindcasts for the two coastal domains were produced using the 3-hourly frequency-direction spectra from the Pt. Arguello (SCB) and Pt. Reyes (GoF) grid points for December–March 1948–1949 to 1997–1998 in conjunction with the gridded transformation functions described above. For the episodes of high waves of concern for these analyses, the use of a single location to characterize the offshore wave environment for an inshore domain, although an approximation, has only minor effects on the results, because latitudinal changes in wave field characteristics over the scales of the inshore domains in such cases are generally small.

Another limitation of the downscaling technique used here is that the calculations do not account for wave generation by winds within the inshore domains. Because the GoF is generally more exposed to the open ocean than the SCB, this limitation has less effect in the former domain. Within the SCB, the lack of wind generation within the domain should have relatively little effect at locations exposed to the open ocean to the northwest and west (where waves propagating into the domain dominate extreme wave climate), but will be important at more sheltered locations where waves generated by strong winds within the Bight (most typically from the northwest, east to northeast, or south to southeast; the direction of importance will depend on the specific location) can reach 2–4 m. The result of this effect will be that in protected inshore regions the mean hindcast extreme waves are biased low, i.e., it should be recognized that (within the SCB especially) the hindcast results are relevant to waves propagating into the domain.

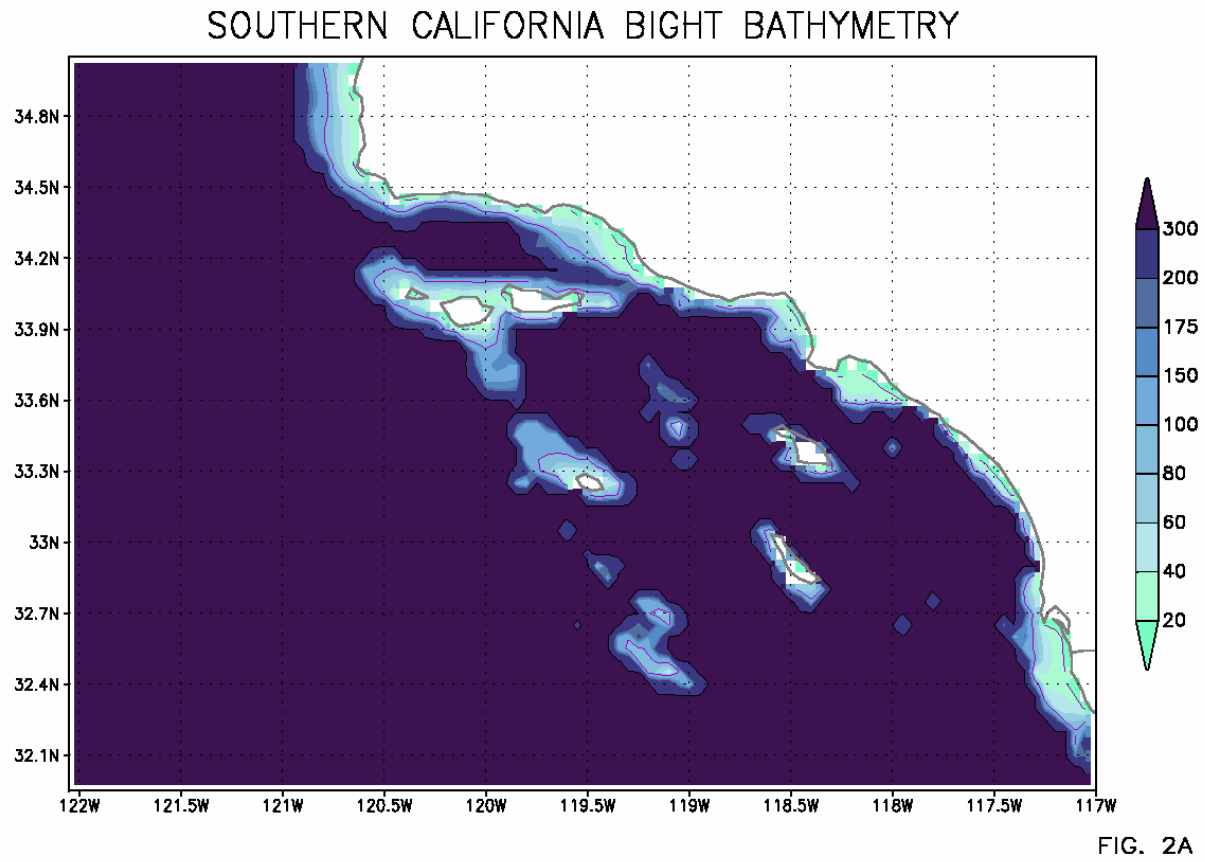

Figure 2A. Bathymetry (meters) in the Southern California Bight domain (line contours at 20,100, and 300 meters).

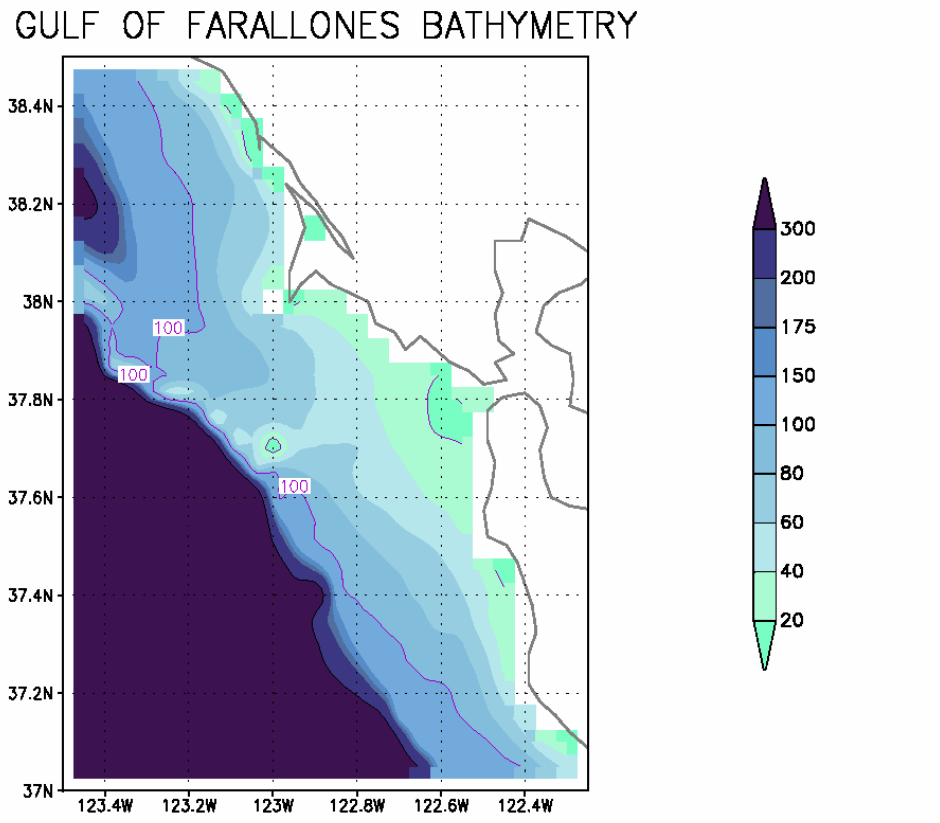

Figure 2B. As in Fig. 2A, but for the Gulf of the Farallones domain.

The hindcast results are described in terms of traditional first- and second-order statistics (means, linear-least square trends) and t-test significance values, so no further description is given here. The text does use some notational conventions for wave statistics as follows:

H_S^{99} (H_S^{95}) – denotes annual 99th (95th) percentile significant wave height (threshold values).

P^{99} – denotes annual average dominant period (dominant period is calculated by the wave model on the basis of the moments of the directional spectra) for those cases where H_S exceeded H_S^{99}.

Θ^{99} – denotes annual average dominate direction (dominate direction is calculated by the wave model on the basis of the moments of the directional spectra) for those cases where H_S exceeded H_S^{99}. The directional values given by the wave model were converted to vector components and averaged without weighting by the corresponding wave energy.

3. Results

3.1 Large-scale Hindcast Results

To establish a background for considering wave climate and wave climate changes over coastal domains, we begin by presenting relevant results from the large-scale hindcast over the North Pacific (see also Wang and Swail, 2001; Graham and Diaz, 2001; Bromirski et al., 2004). Figure 3a shows average December-January-February-March (DJFM) H_S^{99}. The pattern shows wave heights increasing values from south to north across the western North Pacific, with the orientation becoming more southwest-northeast across the eastern ocean. A maximum (10 m) is located between approximately 38˚–48˚N and 175˚E–170˚W. Along the coast of California, mean values of H_S^{99} increase from approximately 4 to 7 m from south to north.

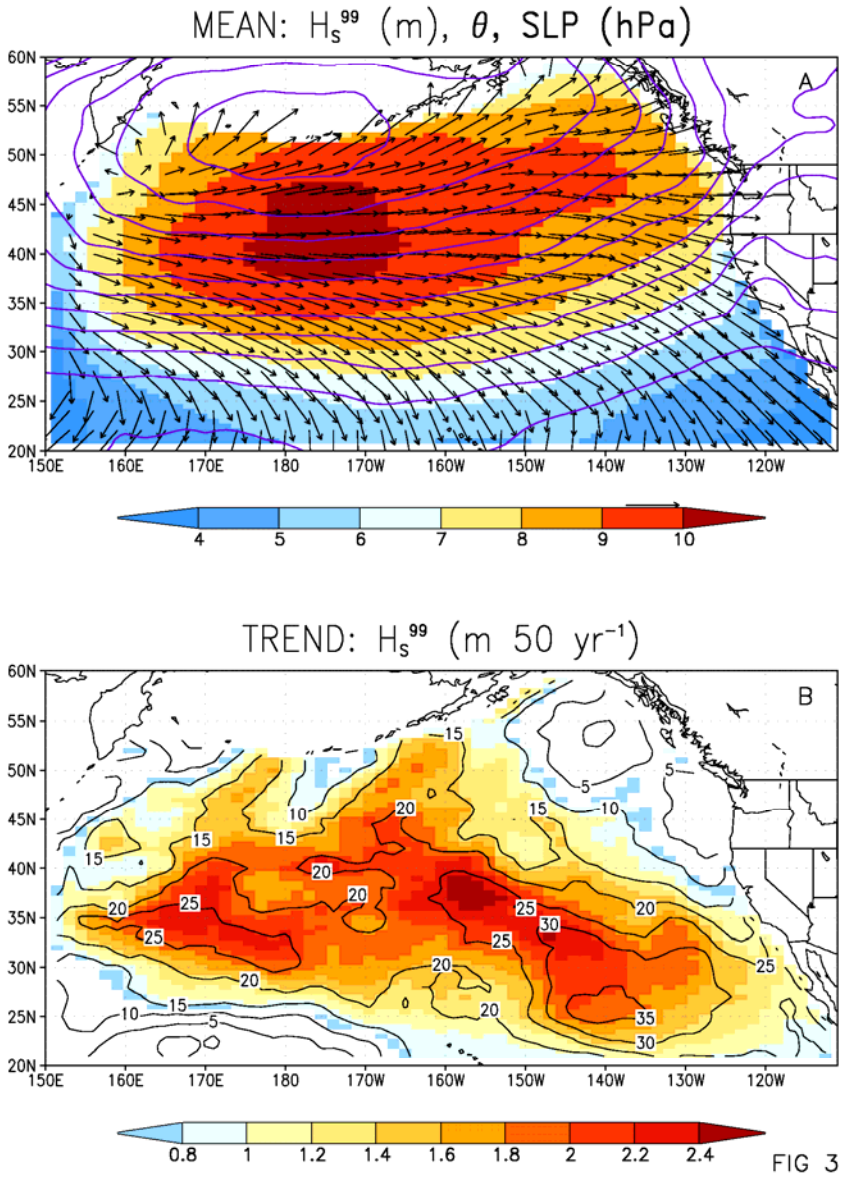

Figure 3. (A) Mean H_S^{99} (m; color), mean θ^{99}, and 1st percentile SLP (contours, contour interval is 4 hectopascals (hPa), lowest value is 964 hPa). (B) Trend in H_S^{99} (m 50 yr^{-1}, color), and expressed as a fraction of mean H_S^{99}. The trend is shown only where t-test significance exceeds the 90% level.

The features in the mean H_S^{99} field can be related to the distribution of mean DJFM first percentile sea level pressure (SLP) (six-hourly NCEP reanalysis data from 1947–1948 to 1997–1998), also shown in Fig. 3a. The SLP field indicates mean west-northwest – east-northeast oriented surface westerlies across much of the North Pacific, with the strongest gradients (i.e., strongest winds) near the region maximum H_S^{99}. The pattern for mean θ^{99} (dominant direction; also Fig. 3a) shows westerly directions along 40˚N (somewhat farther north in the eastern ocean) with more southerly directions to the north and more northerly directions to the south. Along the coast of California, this pattern results in a mean θ^{99} ranging from slightly north of west off Northern California, to northwest off Southern California.

Figure 3b shows the trends in H_S^{99} [after Graham and Diaz (2001), their Fig. 11d]. These trends show increases of 1 to 2.5 meters across much of the mid-latitude northeast Pacific south of 40˚N, these representing increases of 20%–35% of mean H_S^{99} (similar results are obtained for 90th percentile wave heights by Wand and Swail, 2001—see their Fig. 8a). Along the coast of North America, the largest trends in hindcast extreme wave height (about 1 m, 25% of the mean H_S^{99}) are found in southern California and southward into Baja California. Smaller trends in wave height are depicted in the Gulf of Alaska extending southeastward of the coast of the northwest United States. The pattern of trends in Fig. 3b is consistent the cyclone trends noted earlier (stronger cyclones tracking farther south and east south of 40˚N during the late twentieth century) and only slight wind speed trends in the Gulf of Alaska (see Graham and Diaz, 2001 for further discussion).

Figures 4a and 4b show the mean and trend for P^{99}. The mean field shows a maximum (14.5 s) centered along 40˚N between 150˚–180˚W, about 10˚–15˚ W of the maximum for mean H_S^{99}, and the increasing values

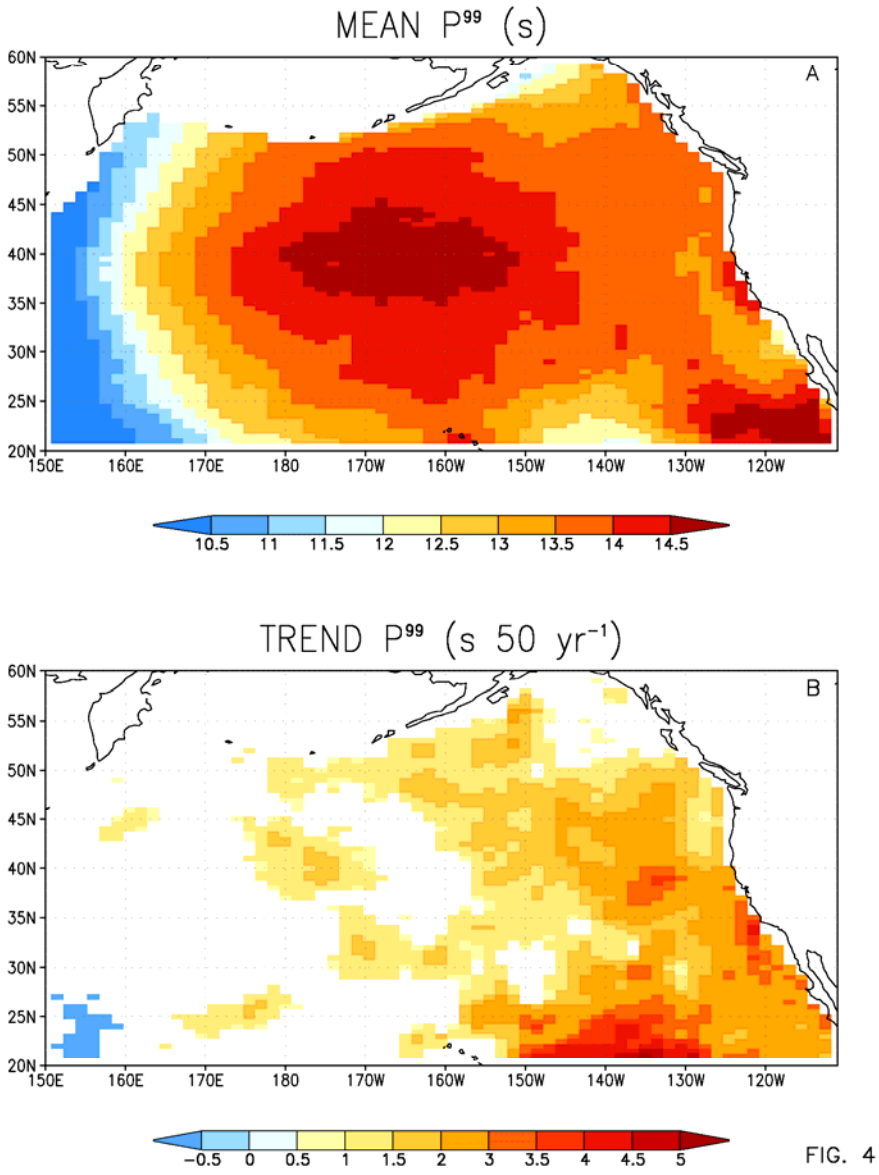

Figure 4. (A) Mean P^{99} (s). (B) Trend in P^{99} (s 50 yr^{-1}), shown only where t-test significance exceeds the 99% level.

along the west coast of North America, particularly from the central California coast southward into Baja California. In the central Pacific, these features largely reflect the character of spectra at relatively short decay distances, with the effects of spectral dispersion and dissipation playing an increasing large role south of 40˚ south, and dominating off the coast of Baja California. The region of lower P^{99} (12-13 s) offshore of California reflects contributions from local strong northwesterly fetches. The trends for P^{99} (Fig. 4b) show positive values nearly everywhere, with increasing values towards the east and south reaching 4.5-5 s 50 yr^{-1} in the region of climatological trade winds between the Hawaiian Islands and 130˚W. Along the coast of California southward from San Francisco, trends in P^{99} are typically 2.5-3.5 s 50 yr^{-1}.

Figure 5 depicts trends in binned (f, θ) energy (m^2) for times when H_S exceeded the 99th percentile at six locations in the eastern and central North Pacific. These locations include the model points listed in Table 1 with the additions of a point off southern Baja California (Cabo San Lucas; 23˚N, 112.5˚W) and off the Oregon-Washington border (denoted Columbia, 46˚N, 126˚W). The trends for the locations along the U.S. West Coast (Pt. Arguello, Pt. Reyes, Buoy 46006, and Columbia) each show a pattern of decreasing energy from northwesterly approach directions at periods of 12.5-15 s, and increasing energy from more westerly directions particularly at periods of 15-17.5 s. The spectral trends at NW Hawaii and Cabo San Lucas are dominated by increases centered at 315˚ and 300˚, and 13-16 s, indicative of the energized storm track along 40˚N.

An EOF analysis was performed using the 95th percentile H_S directional spectra at the six locations discussed above. For this analysis, the binned energy at each location was scaled so that each had the same total variance (thus, each point equal representation in the analysis, but within-point spectral structure is retained). The loadings for the first EOF [49% of the total (scaled) variance] show patterns quite similar to the trends (Fig. 5), emphasizing that the joint variability at these locations is dominated by the trend. On a point-by-point basis, this first EOF accounts for 60% of the variance at Pt. Arguello and Cabo San Lucas, 49% at Pt. Reyes, 45% at Buoy 46006, 43% at Hawaii, and 30%

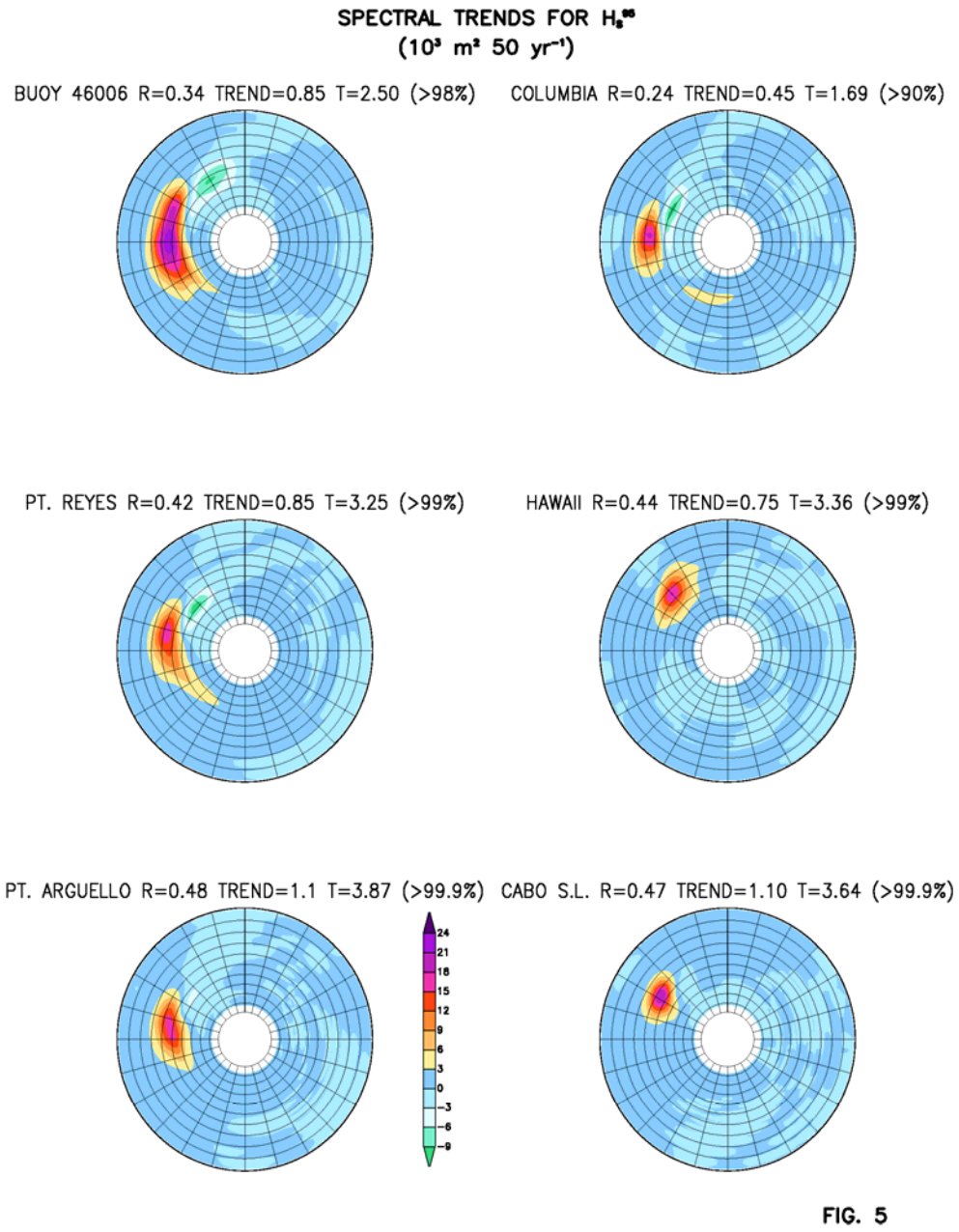

FIG. 5

Figure 5. Trends in frequency-direction spectra (see Table 1 and text for locations) for cases where H_S exceeded the 99th percentile (values are 10^3 m^2 50 yr^{-1}); legends give (A) correlation between trend and time series of H_S^{99}, (B) H_S^{99} trend, t-test for trend significance, and t-test significance level. Spectral roses indicate approach direction (i.e., westerly swell comes from the left), and period (ranging from 0 to 27.5 s from inside to out at 2.5 s increments).

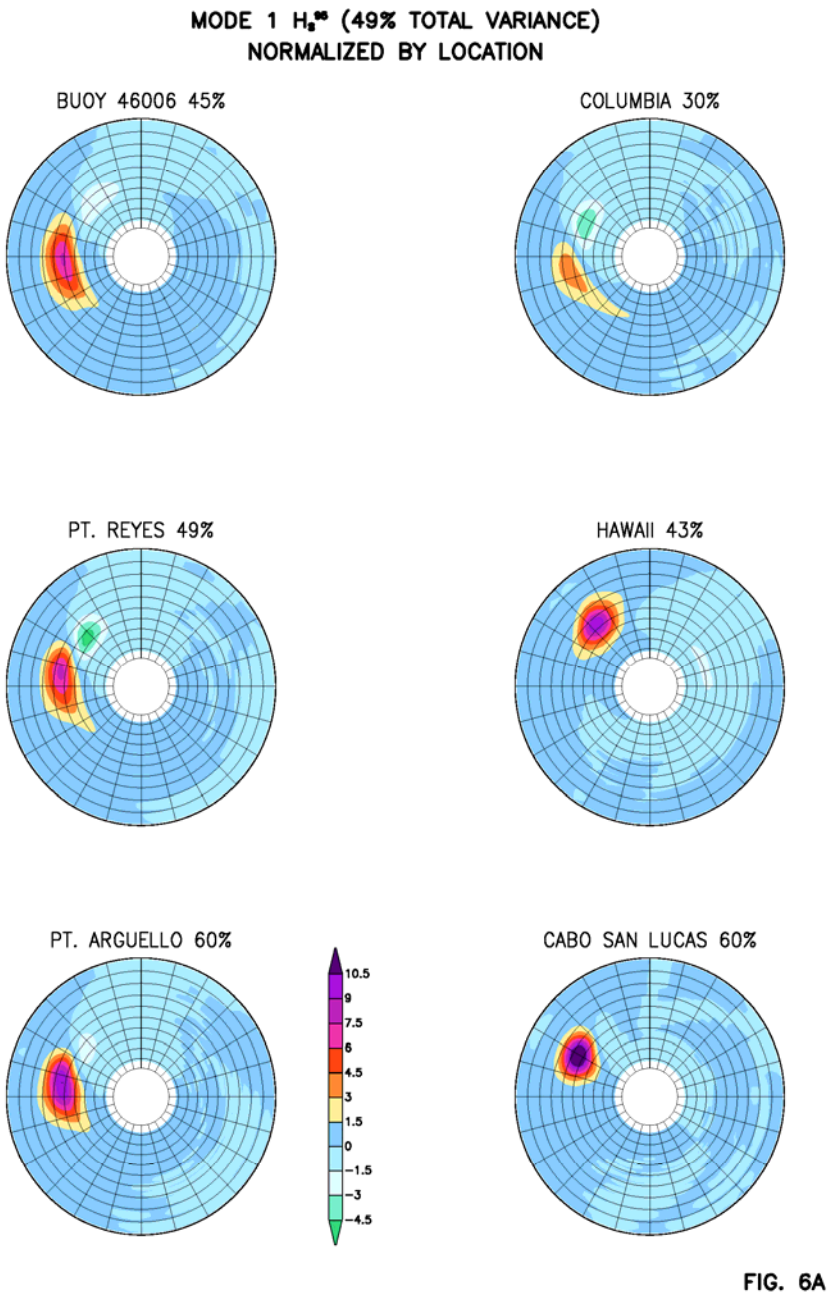

Figure 6A. Loadings for lead EOF of frequency-direction spectra for cases where H_S exceeded 95th percentile (see Table 1 and text). Legends give percent of the variance at each location accounted for by the EOF mode); see Fig. 5 for details concerning axes.

at Columbia (i.e., higher values at locations farther south and east). The temporal function for this EOF (Fig. 6b) shows a strong upward trend with peaks in the late 1950s and late 1970s–early 1980s.

For comparison with the spectral EOF described above, the EOF of gridded H_S^{99} (Fig. 7) shows a spatial pattern much like the trend [Fig. 2b; and very similar to that obtained by Wang and Swail (2001), see their Figure 10]. The temporal functions for the lead EOF of the gridded and spectral data (Fig. 6b) are essentially identical (the correlation is 0.92), a result that emphasizes the pervasive impact on wave climate of the trend in atmospheric circulation (see Wang and Swail for further discussion of this point).

A final analysis using results from the large-scale hindcast deals with the association between ENSO variability and extreme wave heights. This is done by correlating H_S^{95} with DJFM sea surface temperature anomalies (SSTA) in the eastern equatorial Pacific (the NINO3 region, 5˚N-5˚S, 90˚W-150˚W; data from Kaplan et al., 1997). The results (Fig. 8), show a higher correlation in a region extending from north of 40˚N in the central North Pacific to south of 40˚N in the eastern ocean, with maximum correlations (above 0.6) between 130˚W and 140˚W south of 30˚N (note: correlations are higher for median wave heights and smaller for H_S^{99}). Thus, over the period covered by the hindcast, El Niño variability (which, like the PDO, trended irregularly after the late 1940s) accounted for a substantial portion of the variability in extreme wave heights in the eastern North Pacific south of 40˚N. Interestingly, the pattern of NINO3 correlations is similar to the trends in 99th percentile H_S (Fig. 2C) in the eastern ocean, but much different from the trends in the central and western North Pacific (where there are large positive trends south of 40˚N, but where correlations with NINO3 are small or negative). This behavior may relate to the fact that El Niño-related circulation anomalies tend to be centered in the central-east North Pacific (e.g., Trenberth and Hurrell, 1994), while the lower frequency PDO-related pattern has larger zonal scales (e.g., Zhang et al., 1996; Mantua et al., 1997).

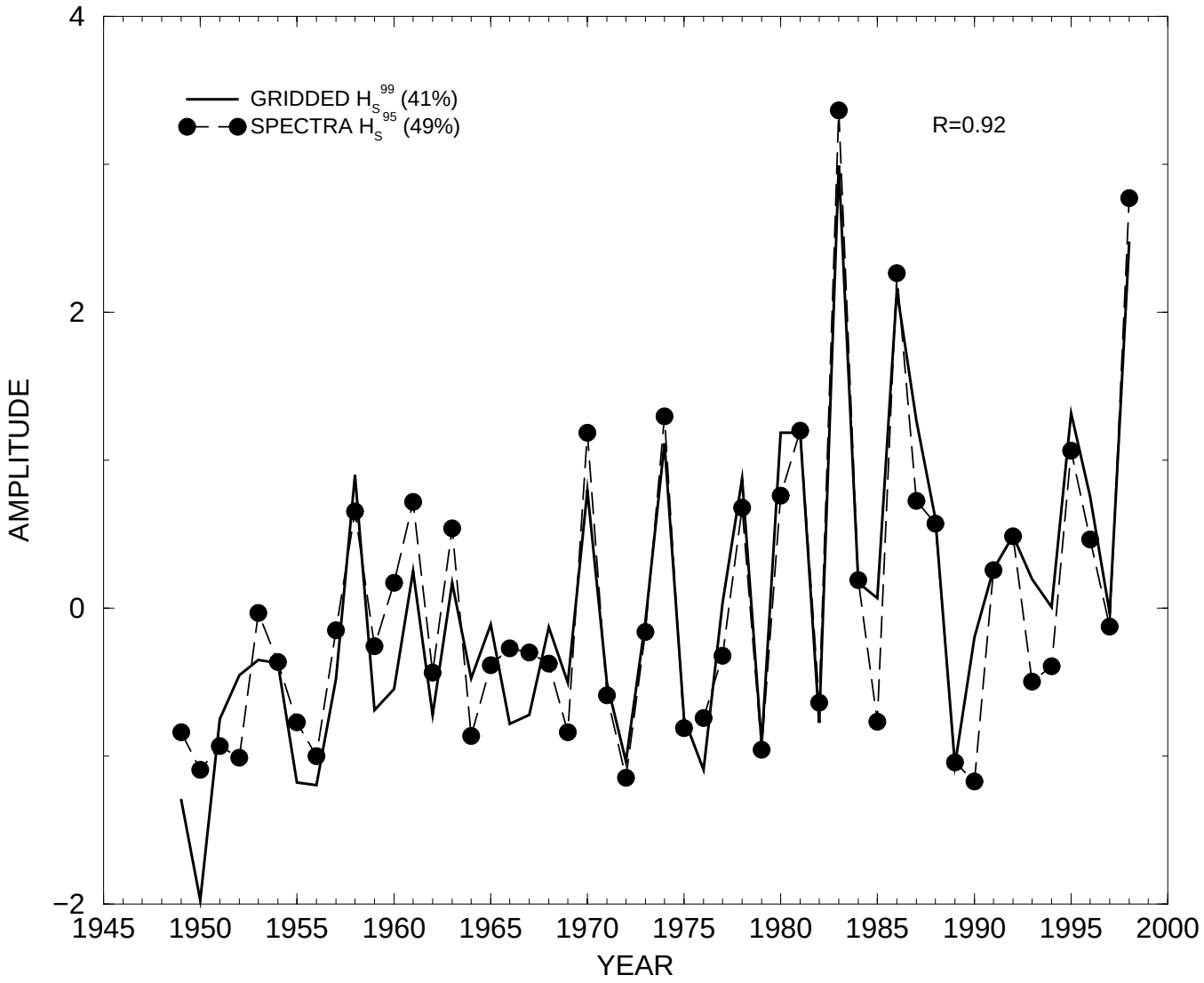

FIG. 6B

Figure 6B. Temporal amplitudes (standardized) for lead EOF of frequency-direction spectra (see Fig. 6A; solid), and for gridded 95th percentile H_S (see Fig. 7).

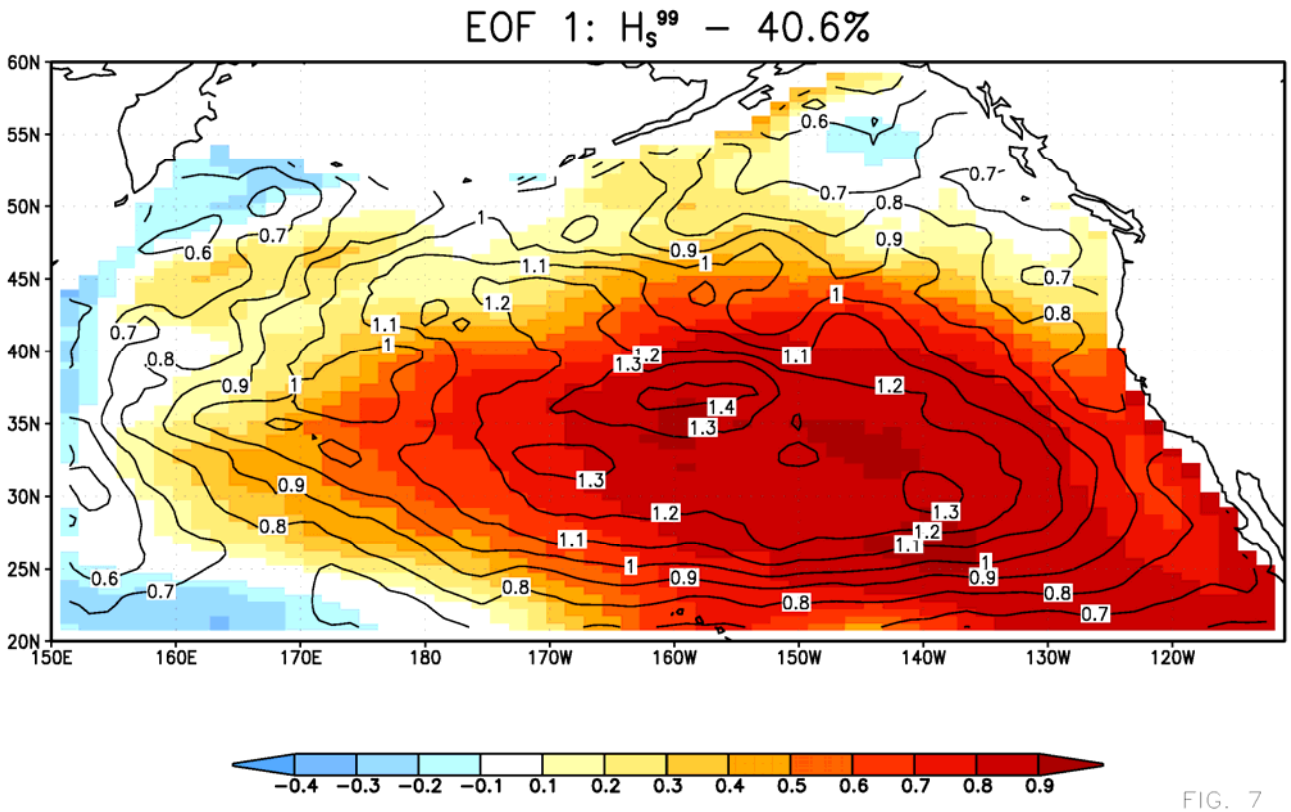

Figure 7. Lead EOF of H_S^{99} (colors – arbitrary units), and trend in first percentile SLP (hPa 50 yr^{-1}).

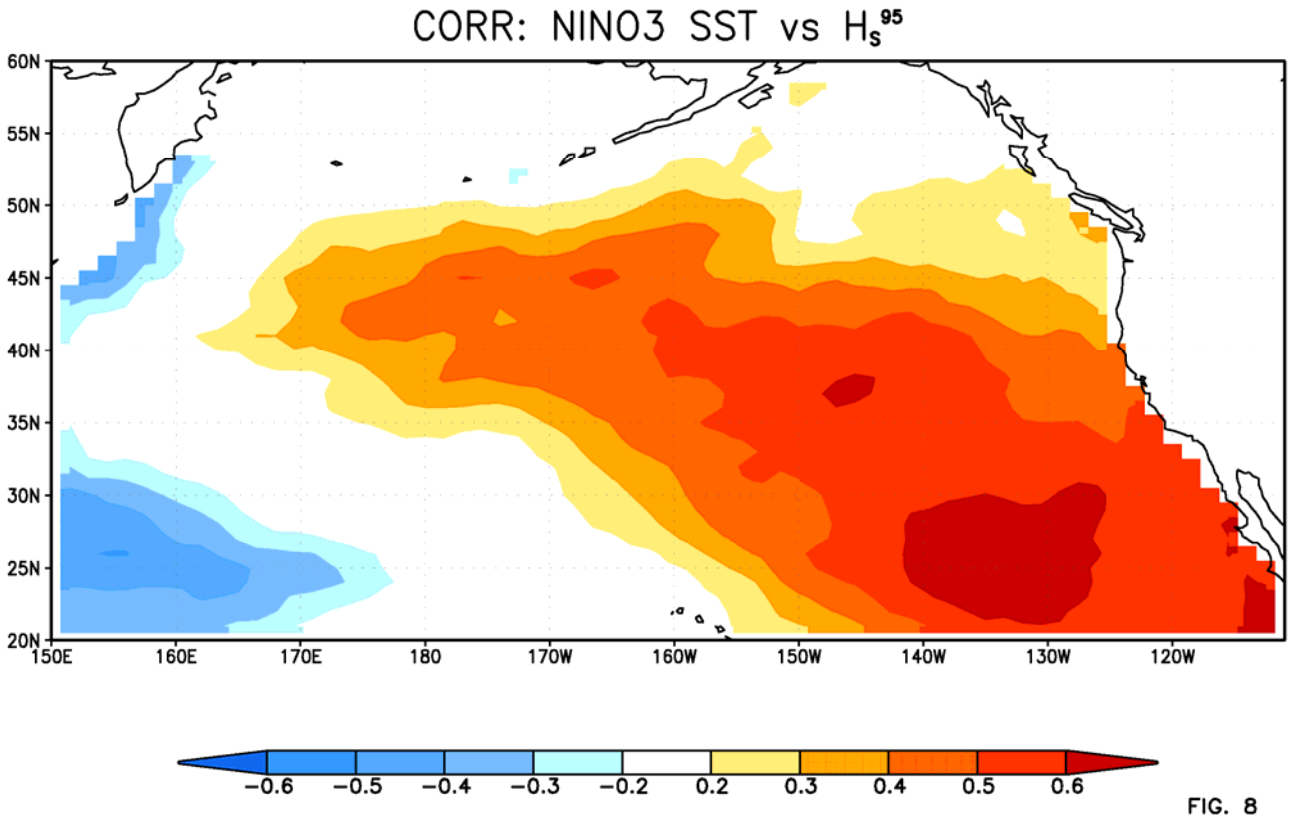

Figure 8. Correlations between NINO3 SSTA and hindcast H_S^{95}.

3.2 Wave Climate Variability along the California Coast

3.2.1 The Southern California Bight

Figure 9a shows mean H_S^{99} for the SCB derived as discussed in Section 2. The favored west-northwest approach direction for large waves entering the bight is clearly evident in the patterns of island sheltering, as well as in the general inshore reduction in height due to sheltering (the dominant effect expect close to coastlines) and refraction. Trends in downscaled H_S^{99} (Fig. 9b; calculated using the bias adjustment noted above) show the effects of both (1) the upwards trend in incident wave energy outside the SCB (Fig. 3b), and (2) the rotation of incident angle for larger waves (Fig. 5; the trend towards longer periods (Figs. 4b and 5) probably plays a role as well but is more difficult to analyze. The impact of the increasing energy approaching from more westerly directions is apparent from the fact that the trends in wave heights are largest in areas sheltered from waves approaching from the northwest and smallest in areas exposed to waves approaching from that direction. This effect is sufficiently large that trends in some inshore regions with some island sheltering islands are larger than in the deep water (untransformed) value. Along the coast, the largest trends (typically 1.0–1.2 m 50 yr^{-1}) are found at the eastern end of the Santa Barbara Channel, from the Malibu coast, through Santa Monica Bay to the Palos Verdes Peninsula, and along the Orange and San Diego county coasts.

To give an idea of the relative magnitude of the trends in Fig. 9b, Fig. 9c shows "normalized trends", i.e. the trend expressed as a fraction of mean H_S^{99}. To assist in interpreting the map of normalized trends, note that if the relative distribution of energy as a function of frequency and direction did not change (i.e., only the total energy changed), the normalized trends would have the same value everywhere. In contrast to this idealized situation, Fig. 9c shows considerable structure, and comparing the pattern with the average values shown in Fig. 9a, it is apparent that (by this measure) the largest (coastal and otherwise) relative trends in H_S^{99} (50%–70%) have been experienced in regions that climatologically have the smallest extreme waves (more protected from the northwest, less protected from the west).

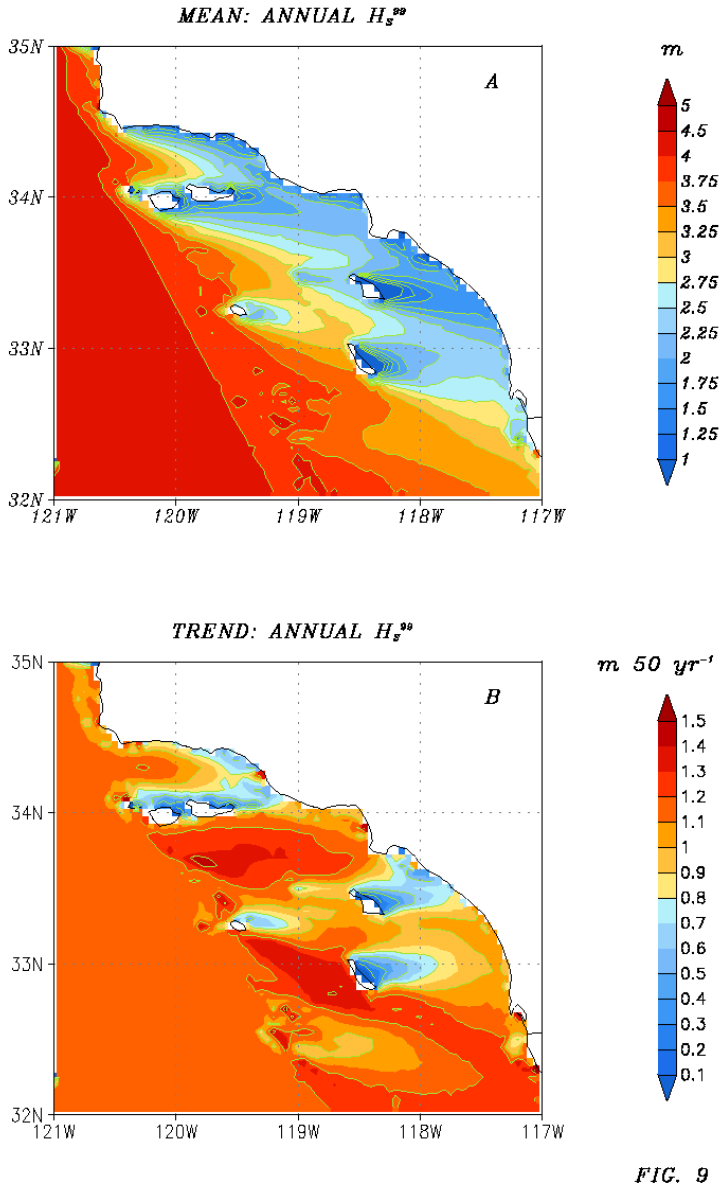

Figure 9. Downscaled hindcast wave data for Southern California Bight. (A) mean H_S^{99} (m), (B) trend in H_S^{99} (m 50 yr^{-1}).

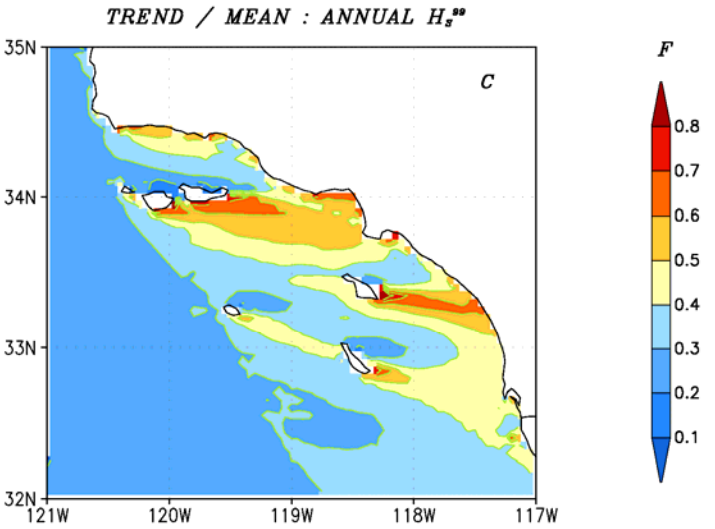

FIG. 9C

Figure 9 cont. (C) trend in H_S^{99} expressed as a fraction of mean H_S^{99}.

Figure 10a shows correlations between annual H_S^{95} and NINO3 SSTA. Moving from the west into the Bight, the correlations are about 0.55 in the open ocean (as in Fig. 8), increasing slightly (to 0.58–0.60) in sheltered outer waters, then decrease (to 0.45–0.55) in the inner waters. The regions of higher correlations in the outer waters of the Bight reflect the more westerly approach directions associated with El Niño-related circulation changes (much as seen in Fig. 9b for the trend), while over inner waters of the Bight, the complicated pattern and lower correlations reflect details of local exposure as changes in incoming wave height, direction, and period alter the effects of sheltering and refraction. To emphasize the relatively impact of El Niño-related variability, Figure 10b shows the ratio between the standard deviation of annual H_S^{95} regressed on NINO3 SSTA (H_S^*) and annual mean H_S^{95}. The pattern is similar to that for the normalized trends (Fig. 9c), with the largest values of H_S^* (up to about 25% of H_S^{95}) being found in areas sheltered from the northwest and exposed to the west-southwest (where average values of H_S^{95} tend to be low), and the smallest values of H_S^* (around 10% of H_S^{95}) in areas exposed to the northwest and protected from the west-southwest. As is the case for the large-scale model results (see discussion of Fig. 8), the correlations (not shown) are lower for more extreme wave heights (e.g., 99th percentile) and considerably higher for the average or median statistics.

3.2.2 Gulf of the Farallones

Figure 11A, corresponding to Fig. 3a (large-scale model) and Fig. 9a (SCB), shows mean annual H_S^{99} for the GoF region. Reflecting the relatively less complex coastal geometry (in comparison to the SCB), the distribution of H_S^{99} over the GoF can be broadly summarized as a reduction from values of just over 6 m in the outer waters to typical values of about 4–4.5 m in the inner waters. This reduction in energy (45%–55%) is commensurate with refraction from typical approach directions (300–315˚) to the typical coastal normal angle of about 250˚. Important details in the distribution of H_S^{99} are protection (due to refraction) from Cordell Banks (west of Pt. Reyes) and the shoals around the Farallone Islands, shoaling and refraction onto the bars off the Golden Gate, and reduced wave heights in the more sheltered coastal strip from Drakes Bay (in the lee of Pt. Reyes) to the Golden Gate. The trends in H_S^{99} (Fig. 11B) show values of

about 0.7 m 50 yr^{-1} in the outer waters, with larger values (typically 1–1.2 m 50 yr^{-1}) widely distributed through the inner waters south of Pt. Reyes. As was the case for the SCB, some of this detail is due to the trend towards more westerly approach directions (Fig. 5; in particularly the larger trends southwestward from Pt. Reyes and from the Farallones). Details of refraction patterns and the trend towards increasing wave period (additional shoaling) likely contribute as well but require more detailed analysis to describe. In terms of the relative trend (Fig. 11C; the trend in H_S^{99} divided by mean H_S^{99}, as in Fig. 9c), values are smaller than in the SCB, largely because the offshore values in the GoF are smaller (smaller trends and larger mean values of offshore H_S^{99}). The largest relative trends (typically 20%–25%) are along the southwest-facing coast from Pt. Reyes to just north of the Golden Gate, and just south of the Golden Gate (Ocean Beach). As in the SCB, these features appear to result mostly from the rotation in preferred approach direction, and the net effect is to produce the largest relative changes in the climatologically most protected stretches of coast.

Correlations between H_S^{99} and El Niño for the GoF (Fig. 12a) show mostly smaller values than in the SCB (consistent with the open ocean correlations decreasing towards from south to north), and as again show larger values in the outer waters (typically 0.45–0.50) than in inshore regions (typically 0.4–0.45). As was the case for the SCB, the pattern of correlations in Fig. 12A is complex, but it is apparent that areas with less refractive / sheltering effects tend to have higher correlations, suggesting that the sensitivity of those effects (i.e., in more protected areas) to specifics of incoming wave periods and approach direction tend to reduce systematic relationships with the changing open ocean wave conditions (i.e., reducing the covariance). Consistent with the lower correlations and larger mean H_S^{99}, the magnitudes of the relative El Niño signal (Fig. 12; the ratio H_S^* to mean H_S^{99}, as in Fig. 10b), are considerably smaller than in the SCB. As they were for the relative trends, the largest values (0.09–0.12) are depicted from Drakes Bay to just south of the Golden Gate. Elsewhere, there is a clear pattern for larger values along the coast, likely due to the trend towards for more westerly approach directions (less refraction) and longer periods (more shoaling) during El Niño episodes.

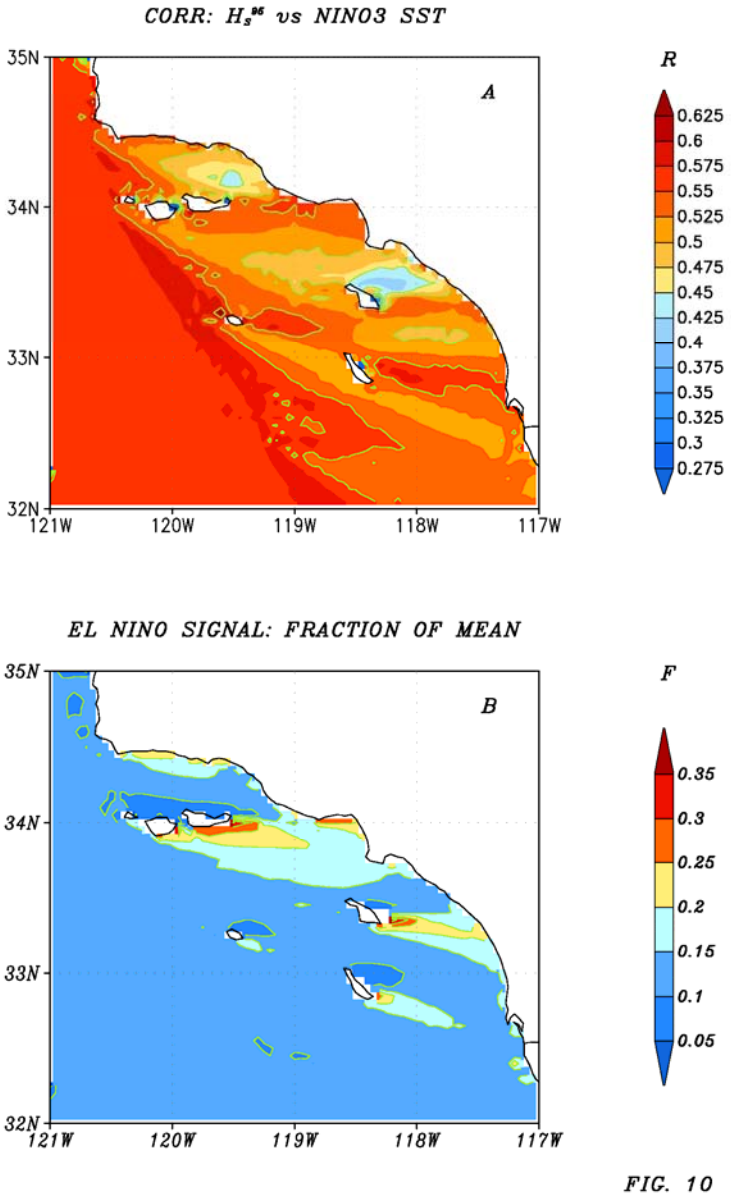

Figure 10. (A) Correlations between annual H_S^{95} and NINO3 SSTA for the Southern California Bight. (B) Standard deviation of regressed H_S^{95} from NINO3 SST expressed as a fraction (F) of mean H_S^{95}.

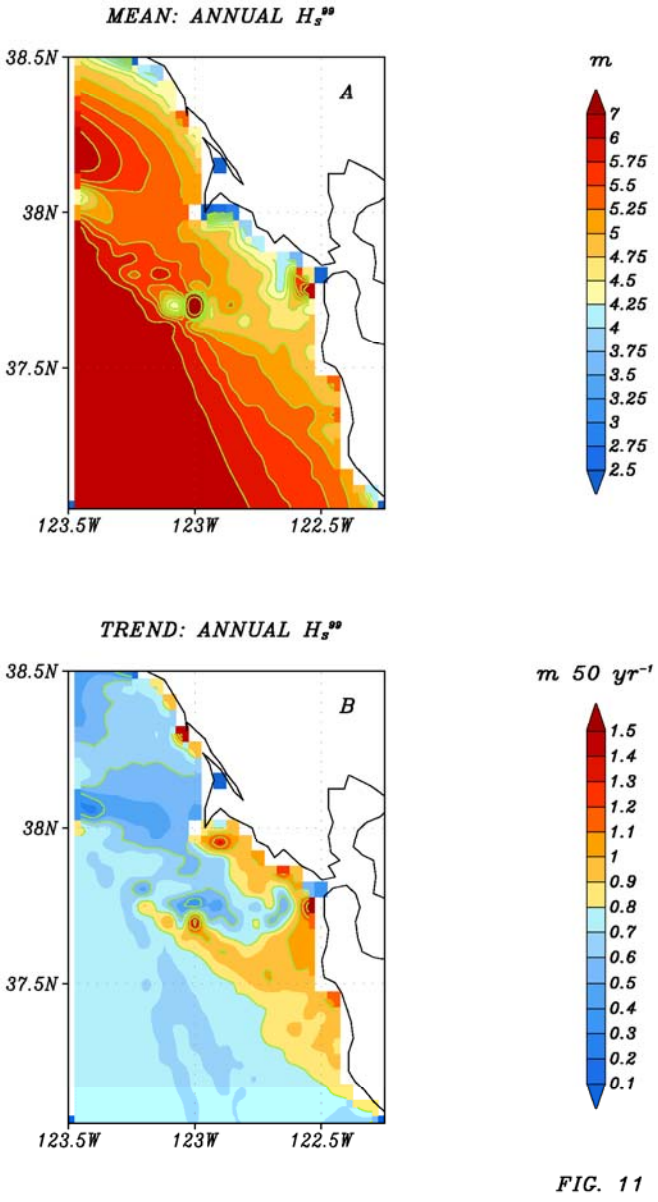

Figure 11. As in Fig. 9A,B, but for the Gulf of the Farallones.

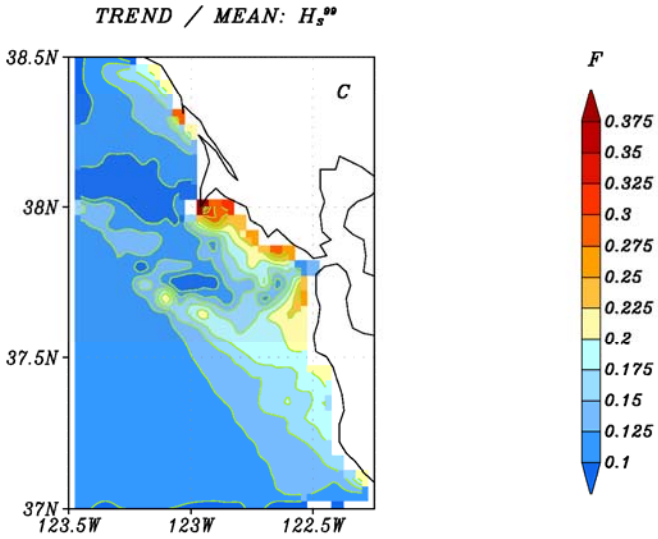

FIG. 11C

Figure 11 cont. (C) trend in H_S^{99} expressed as a fraction of mean H_S^{99}.

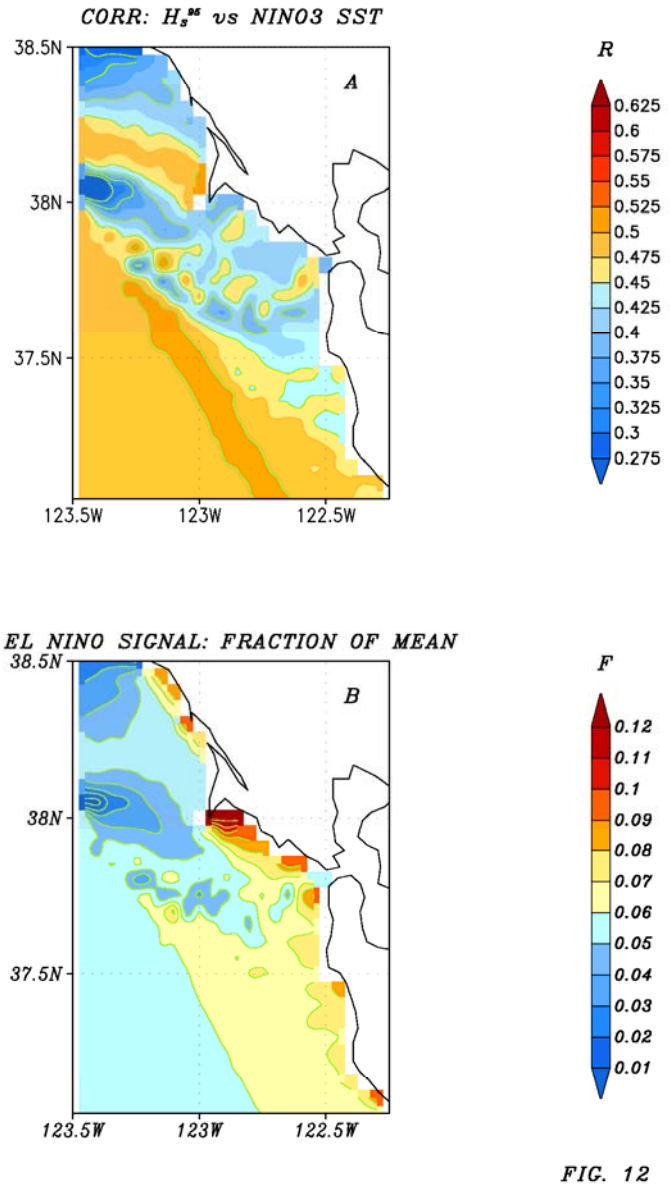

Figure 12. As in Fig. 10, but for the Gulf of the Farallones.

4. Summary

Results from a 50-year winter wave model downscaling simulations for domains covering the Southern California Bight and the Gulf of the Farallones on the California Coast have been described. Downscaling was performed using direction-frequency transformation functions derived using the model of O'Reilly (1991) at a resolution of approximately 5 km. The forcing for the downscaling simulations come from directional wave spectra for points off these two domains taken from a large-scale winter wave hindcast for the North Pacific forced with NCEP reanalysis winds (Graham and Diaz, 2001). Agreement between approximately 20 years (winters) of contemporaneous 3-hour simulated and measured H_S at two locations along the California coast is quite good, with correlations at the two forcing locations of 0.85 and 0.88 for Pt. Arguello and Pt. Reyes, respectively. The results for Pt. Arguello from the large-scale model do show a slight low bias in H_S. This feature, thought to be representative of conditions along the immediate coast of central California and offshore Southern California, is due to low bias in the reanalysis winds and details of the implementation of the wave model. In addition, because the effects of wave generation by winds within the domains is ignored, the downscaling approach is expected to produce low biases at some more protected areas in both the SCB and GoF regions (less in the latter, owing to its greater exposure).

Results from the large-scale model show the following two main features that are of particular relevance to the coast of California:

1. There is a substantial upward trend in H_S^{99} over the eastern North Pacific (up to 2.4 m 50 yr^{-1} and 35% of the average) during the last half of the twentieth century, with associated trends towards longer periods waves and more westerly (less northwesterly) approach directions. Along the coast of North America, the largest trends in H_S^{99} and P^{99} are found along the coast of central and southern California and into Baja California. An analysis of the relationship between winter hindcast wave heights and El Niño variability showed correlations (up to 0.6) between winter mean extreme (95th percentile) H_S and NINO3 SST in much of

the eastern North Pacific, especially south of 40˚N and east of 150˚W. Correlations between hindcast wave heights and NINO3 SST are higher for lower cut-off statistics (e.g., the median) and lower for higher cut-off statistics (e.g., the 99th percentile).

2. Both the trend and interannual variability in hindcast H_S^{99} statistics show strong spatial and spectral coherence across the eastern North Pacific at scales commensurate with low-frequency changes in seasonal atmospheric circulation and cyclone characteristics (reprising in part the results of Wang and Swail, 2001 and Graham and Diaz, 2001; c.f. Allan and Komar, 2000; Bromirski et al., 2004).

For the downscaling results in the Southern California Bight, the trends in H_S^{99} show considerable structure associated with the convolution of mainland and island sheltering and the trends towards higher waves propagating into the Bight and more westerly approach directions. Relative trends (the trends divided by long-term mean H_S^{99}) show values of 40% over most of the inner waters of the Bight, with the largest values (up to 60% of the mean) in areas that are climatologically more sheltered from the northwest, i.e., areas having smaller long-term mean H_S^{99}. Correlations with NINO3 SST show a general tendency to decline, going from deep water (where the correlation is approximately 0.55) into the inner waters of the Bight, where values (typically around 0.5) are distributed in a complex pattern. Much as was found for the trend (and for similar reasons relating to approach direction), the relative size of El Niño-associated variability in H_S^{99} (the standard deviation of H_S^{99} divided by long-term mean H_S^{99}) is largest (typically 20%–25%) in areas more protected from the northwest, i.e., with generally smaller mean values.

In comparison to the SCB, the bathymetry and coastal geometry of the GoF are less complicated, the exposure to large waves approaching from the northwest is more open, trends in deep water H_S^{99} are smaller, and correlations with El Niño variability lower. All of these factors combine to produce an inshore wave environment that more closely resembles offshore conditions and with less fine-scale structure than in the SCB.

Nevertheless, the combined effects of changing approach directions (and possibly increasing periods) place the largest trends in H_S^{99} (typically 1–1.2 m 50 yr^{-1}) in the inshore waters (in comparison with offshore values of 0.6–0.8 m 50 yr^{-1}), generally in locations facing more to the south. These larger trends represent up to about 25% of mean H_S^{99} along the southwest facing coast from Point Reyes southward to the Golden Gate, and along Ocean Beach (just south of the Golden Gate). Correlations with El Niño variability range above 0.5 in the outer waters and, as in the SCB, tend to decline (to typical values of 0.4 to 0.45) in the inner waters of the domain. As with the relative trend, the relative magnitude of the El Niño signal is largest from Pt. Reyes south to the Golden Gate (with typical values of about 0.10–0.12, about half the near-shore values in protected areas of the SCB).

These results emphasize the importance of considering details of the changes in offshore wave climate when seeking to understand changes along California coastlines. Hopefully, the findings can be usefully related to observed patterns of shoreline variability and assist in guiding coastal planning and management.

5. References

Allan, J. C. and P. D. Komar, 2000: Are ocean wave heights increasing in the eastern N. Pacific?, Eos, Transactions, American Geophysical Union, 47, 561-567.

Bromirski, P. D., D. R. Cayan, R. E. Flick, 2004: Wave spectral energy variability in the Northeast Pacific Ocean, J. Geophys. Res, in press.

Caires, S., A. Sterl, J.-R. Bidlot, N. Graham, and V. Swail, 2004: Intercomparison of Different Wind-Wave Reanalyses. J. Climate, 17, 1893-1913.

Graham, N. E. and H. Diaz, 2001: Evidence for intensification of North Pacific winter cyclones since 1948, Bull. Amer. Met. Soc., 82, 1869-1893.

Gutzler, D. S. and J. M. Wallace, 1981: Teleconnections in the Geopotential Height Field during the Northern Hemisphere Winter Season, Mon. Weather Rev., 109, 784-812.

Haber, J., F. Zeilfelder, O. Davydov and H.-P. Seidel, 2001: Smooth approximation and rendering of large scattered data sets, in “Proceedings of IEEE Visualization 2001”, (T. Ertl, K. Joy and A. Varshney, Eds.), pp.341-347, 571, IEEE Computer Society.

Kalnay, E., M. Kanamitsu, R. Kistler, W. Collins, D. Deaven, L. Gandin, M. Iredell, S. Saha, G. White, J. Woollen, Y. Zhu, M. Chelliah, W. Ebisuzaki, W. Higgins, J. Janowiak, K. C. Mo, C. Ropelewski, J. Wang, A. Leetmaa, R. Reynolds, R. Jenne, and D. Joseph, 1996: The NMC/NCAR 40-Year Reanalysis Project, Bull. Amer. Meteor. Soc., 77, 437-471.

Kaplan, A., M. A. Cane, Y. Kushnir, B. Blumenthal, and B. Rajagopalan, 1997: Analysis of global sea surface temperature 1856-1991, J. Geophys. Res., 101, 22599-22617.

Mantua, N. J., S. R. Hare, Y. Zhang, J. M. Wallace and R. C. Francis, 1997: A Pacific interdecadal oscillation with impacts on salmon production, Bull. Amer. Met. Soc., 78, 1069-1079.

O'Reilly, W., 1991: Modeling surface gravity waves in the Southern California Bight, Ph. D. dissertation, Scripps Institution of Oceanography, La Jolla, CA, 92093, 90 pp.

Tolman, H. L., 1999; User manual and system documentation of WAVEWATCH III, version 1.18, U. S. Dept. of Commerce, NOAA, NWS, NCEP, Ocean Modeling Branch Contribution 166, 4700 Silver Hill Road, Mail Stop 9910, Washington, D. C. 20233-9910, 112pp.

Trenberth, K. E., and J. W. Hurrell, 1994: Decadal atmosphere-ocean variations in the Pacific, Clim. Dyn., 9, 303-319.

Trenberth, K. E., and T. J. Hoar, 1996: El Niño and global change, Geophys. Res. Let., 24, 3057-3060.

Wang, X. L., and V. R. Swail, 2001: Changes in extreme wave heights in the Northern Hemisphere Oceans and related atmospheric circulation regimes, J. Climate, 14, 2204-2221.

Zhang, Y., J. M. Wallace, and M. Iwasaka, 1996: Is climate variability over the North Pacific a linear response to ENSO, J. Clim., 9, 1468-1478.